Electronic Supplementary Material (ESI) for Journal of Materials Chemistry A.

Supplementary information

Exactly regulated copper catalysts exploiting isolated photoelectrochemical reduction of cuprous oxides and random mesh-structured TiO_2 for enhanced photoelectrochemical CO_2 conversion

Shin Young Oh[1,a], Dong Su Kim[1,a,b], Hak Hyeon Lee[a], Kun Woong Lee[b], Ji Hoon Choi[a], Won Seok Yang[a], Young Su Choi[a], Dong Wook Kim[a], Jee Won Byeon[a], Ho Seong Lee[c], and Hyung Koun Cho[,a,b]*

[a] School of Advanced Materials Science and Engineering, Sungkyunkwan University, 2066, Seobu-ro, Jangan-gu, Suwon-si, Gyeonggi-do, 16419, Republic of Korea

[b] Research Center for Advanced Materials Technology, Sungkyunkwan University (SKKU) 2066 Seobu-ro, Jangan-gu, Suwon, Gyeonggi-do, 16419, Republic of Korea

[c] Department of Materials Science and Metallurgical Engineering, Kyungpook National University, 80, Daehak-ro, Buk-gu, Daegu, 41566 Korea

[1] Shin Young Oh and Dong Su Kim contributed equally to this work

[*]Corresponding author. Tel.: +82 31 290 7364

E-mail: chohk@skku.edu

Experimental Section

Cu_2O thin film using electrodeposition:

The substrate was a 180 nm ITO (10-15 Ω $sq.^{-1}$) conductive film with glass. On top of this, a Cu_2O layer was formed in an area of only 20 mm × 30 mm by taping. Before electrodeposition, the ITO was cleaned with acetone, ethanol, and distilled water for 20 min each via sonication. Cu_2O was prepared via cathodic electrodeposition using a three-electrode system consisting of a bilayer including a seed layer. Ag/AgCl (saturated 3 M KCl) and Pt mesh (2.5 cm × 2.5 cm) were used as the reference and counter electrodes, respectively. A seed layer (Cu_2O:Sb) of 200 nm thickness was preferentially formed. The chemical solution was prepared using 0.4 M copper sulfate ($CuSO_4$, Junsei, >98%) and 3 M lactic acid solution ($C_3H_6O_3$, 85% aqueous solution) in distilled water (18 Ω) and adjusted to pH 10 using 4 M sodium hydroxide (NaOH, Sigma-Aldrich) at 60 °C. Then, 3 mM antimony sulfate ($Sb_2(SO_4)_3$, Sigma-Aldrich, >98%) was doped to form a seed layer. Electrodeposition was performed at -0.5 V vs. Ag/AgCl until reaching −0.16 C cm^{-2}. Then, the undoped Cu_2O was formed on the seed layer at pH 11, -0.5 V vs. Ag/AgCl until reaching −1.5 C cm^{-2}.

Atomic layer deposition of TiO_2:

TiO_2, an RM TiO_2 protective layer, was deposited via atomic layer deposition (ALD). The precursor consists of tetrakis (dimethylamino)titanium in a 75 °C chamber and H_2O as an oxygen source at room temperature. Ti Precursor 0.3 s pulse, Oxygen Precursor 0.1 s pulse, and 20 s pause were configured as one cycle. To deposit 2.5 nm TiO_2, 40 cycles were performed under an Ar flow of 800 sccm, 150 °C. In the case of 10 nm TiO_2, the same method was used for 160 cycles.

***Formation of Cu catalyst*:**

The Cu catalyst made on Cu_2O is made from each of HER and CO_2RR solutions and is formed electrochemically using a three-electrode system. Each solution was run under the same conditions at pH 7. 0 V vs. RHE was applied continuously to form the Cu catalyst.

(Photo-)electrochemical measurement:

The PEC CO_2RR experiments were conducted in a saturated 0.5 M $KHCO_3$ solution (pH 6.8) using an H-type cell. The three-electrode system consisted of a working (as-prepared photocathode sample), reference (saturated 4 M KCl Ag/AgCl), and counter electrode (Pt mesh) and was characterized with the Princeton Applied Research Versa STAT 4 system under a 150 W xenon lamp calibrated with an AM 1.5 Filter. Linear scan voltammetry (LSV) and chronoamperometry (CA) were performed under photo on/off and chopped conditions.

Characterization of photocathodes:

Field-emission scanning electron microscopy (SEM; JSM-7600F, JEOL) and transmission electron microscopy (TEM; JEM-2100F, JEOL) were used to analyze the morphology and structure of the Cu_2O-based photocathodes. Patterns were obtained by X-ray diffraction (XRD; Bruker AXSD8 Discover with a Cu Ka radiation source). The optical characteristics of the film samples were analyzed using an ultraviolet-visible (UV-Vis) spectrophotometer (Cary 5000, Agilent Technologies). Surface chemical variations were confirmed using X-ray photoelectron

spectroscopy (XPS, NEXSA, Thermo Fisher Scientific). Copper ion extraction was detected using an inductively coupled plasma-optical emission spectrometer (ICP-OES; Agilent 5100, PerkinElmer AVIO). Time-resolved photoluminescence (TRPL) measurements were conducted using an inverted-type scanning confocal microscope with a 40× objective and 375 nm laser (TRPL, MicroTime-200, Picoquant).

Product analysis:

Hydrogen and Carbon monoxide were detected by gas chromatography (GC, 7890B, Agilent, with 9 ft 1/8 2 mm Molsieve 5A 80/100 UM columns and 6 ft 1/8 2 mm Porapak Q 80/100 SS columns) under 1-sun illumination. H-type cells isolated through a membrane were used. Quantitative analysis of the products was conducted using standard gas.

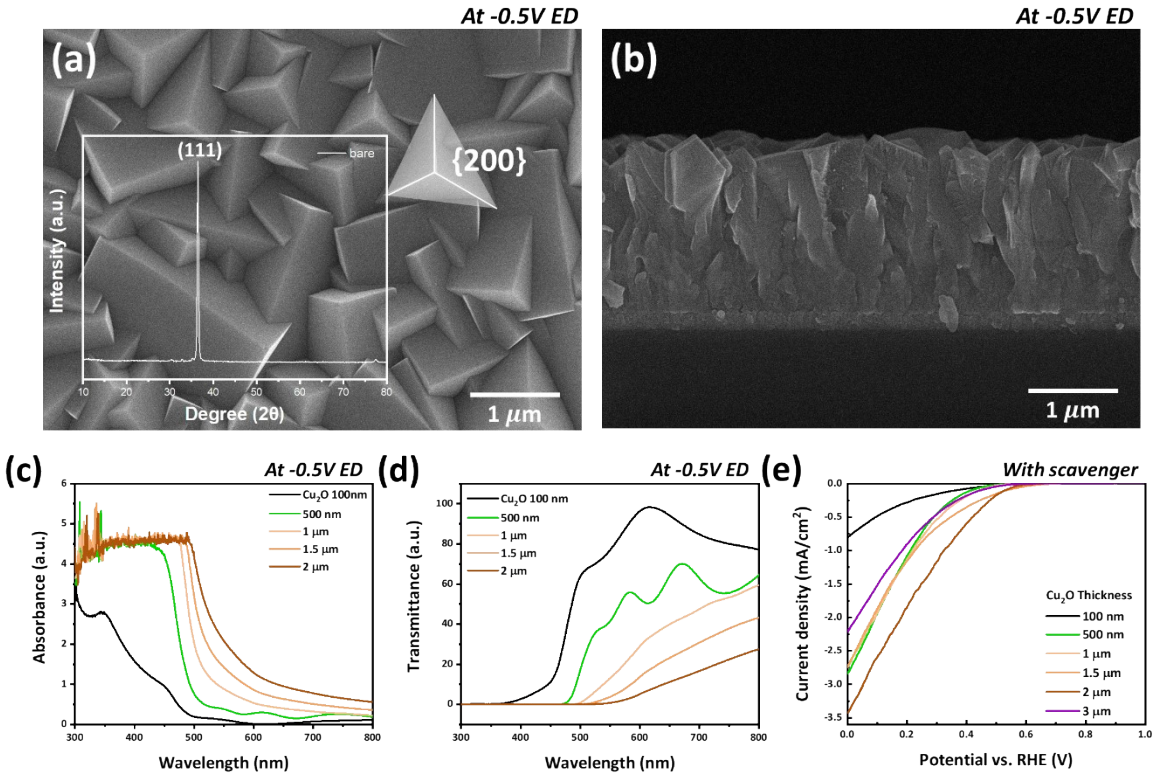

Fig. S1 Properties of electrodeposited Cu_2O. (a) X-Ray diffractometer (XRD) and scanning electron microscopy (SEM) top image of bare Cu_2O and (b) SEM cross image. (c) Absorbance and (d) transmittance analyses. (e) LSV profile of the CO_2 electrolyte with a scavenger for thicknesses of 100 nm, 500 nm, 1 µm, 1.5 µm, 2 µm, 3 µm (−0.5 V vs. Ag/AgCl).

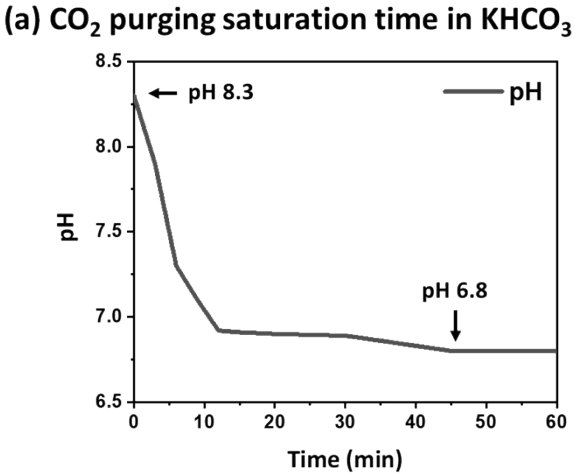

Fig. S2 (a) Change in the pH of 0.5 M saturated $KHCO_3$ solution as a function of CO_2 gas purging time.

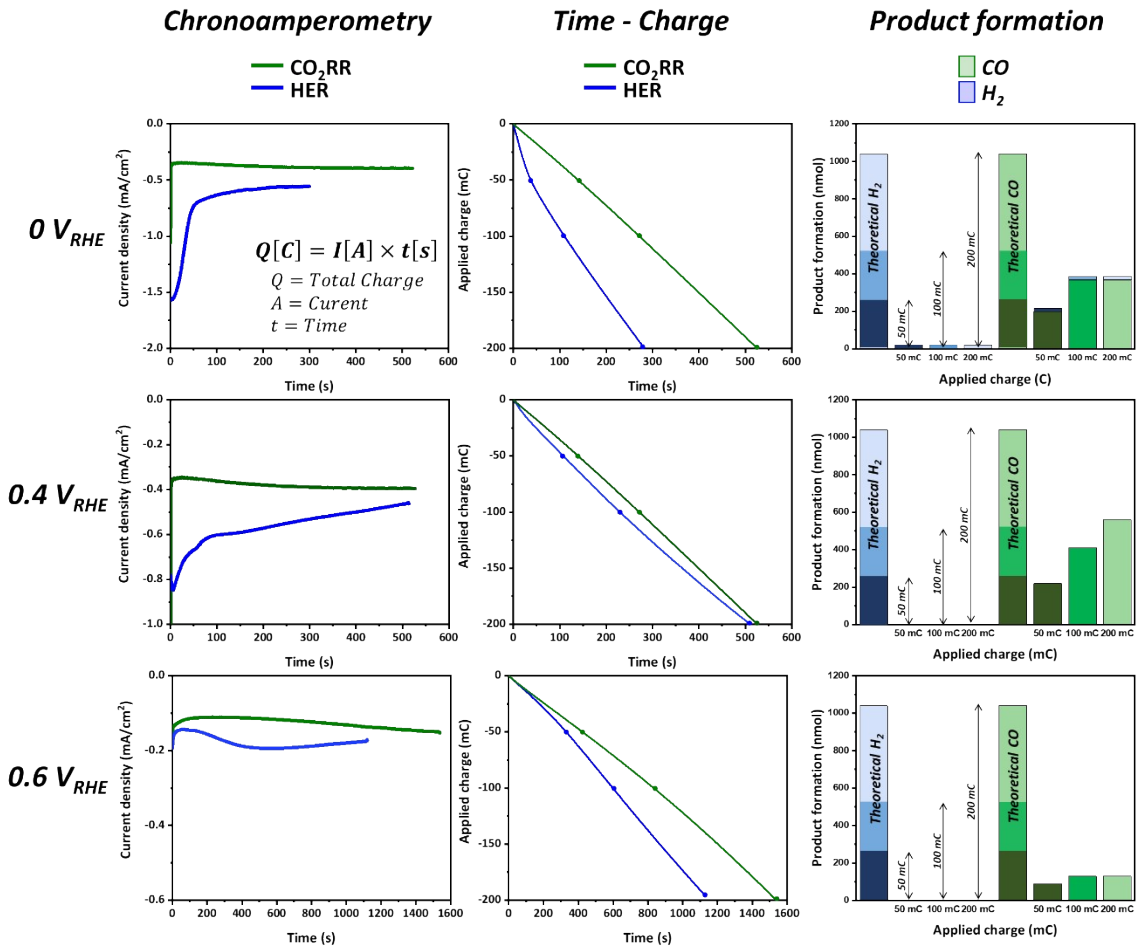

Fig. S3 Chronoamperometry (left side), Q-t (middle side), and product formation (right side) according to potential (0 V, 0.4 V, 0.6 V_{RHE}). Blue: HER solution, Green: CO_2RR solution.

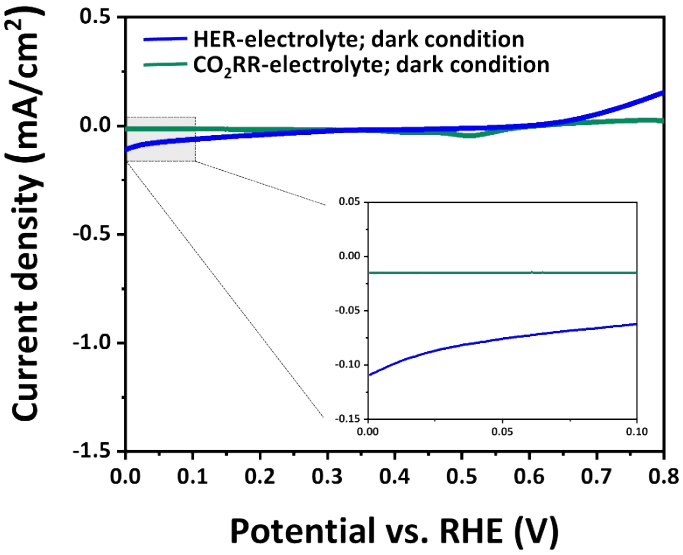

Fig. S4 Linear sweep voltammetry (LSV) curve of Cu_2O in 0.5 M $KHCO_3$ under dark conditions with a scan rate of 10 mV s^{-1}. In HER solution (blue line) and CO_2RR solution (Green line). The inset graph is an enlargement of the gray box area.

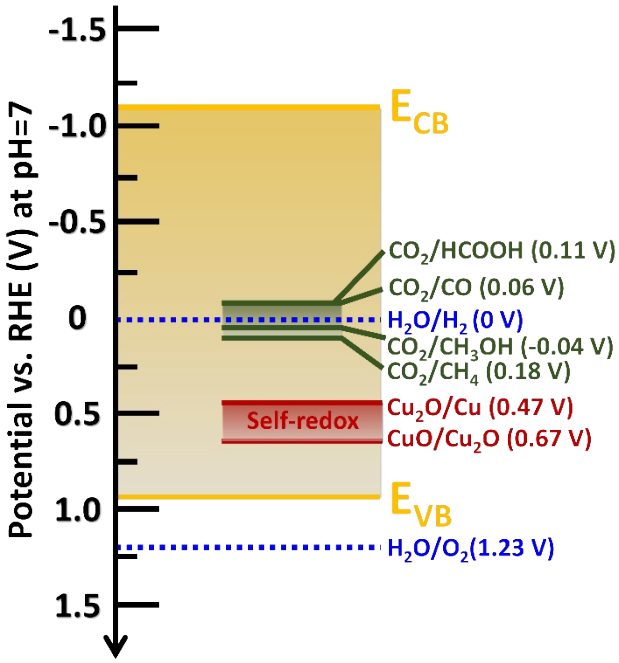

Fig. S5 Schematic of Cu_2O band level at pH 7, including water splitting (blue), CO_2 reduction reaction (green), and self-redox reaction (red) state.

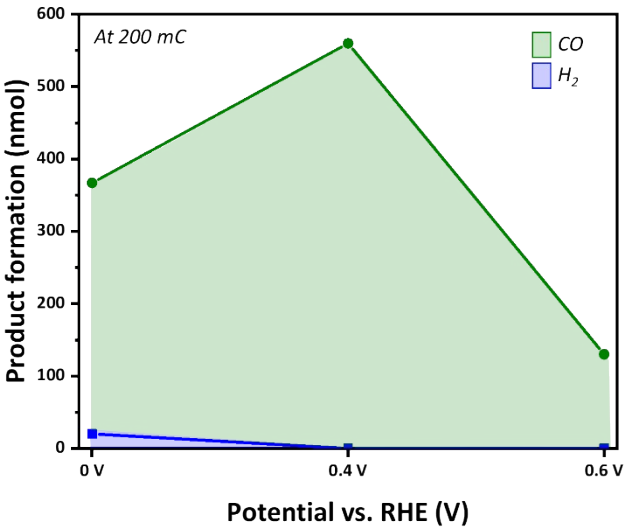

Fig. S6 Amount of H_2 in HER solution (blue) and CO in CO_2RR solution (green) according to potential (0 V_{RHE}, 0.4 V_{RHE}, 0.6 V_{RHE}) up to 200 mC.

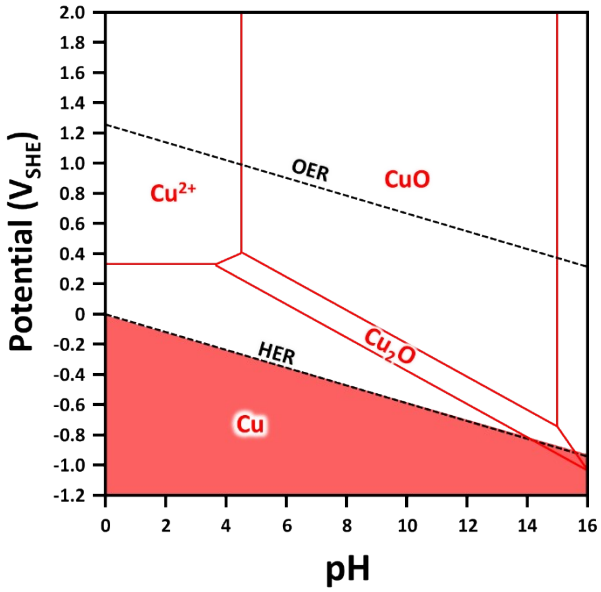

Fig. S7 Pourbaix diagram of Cu-based materials.

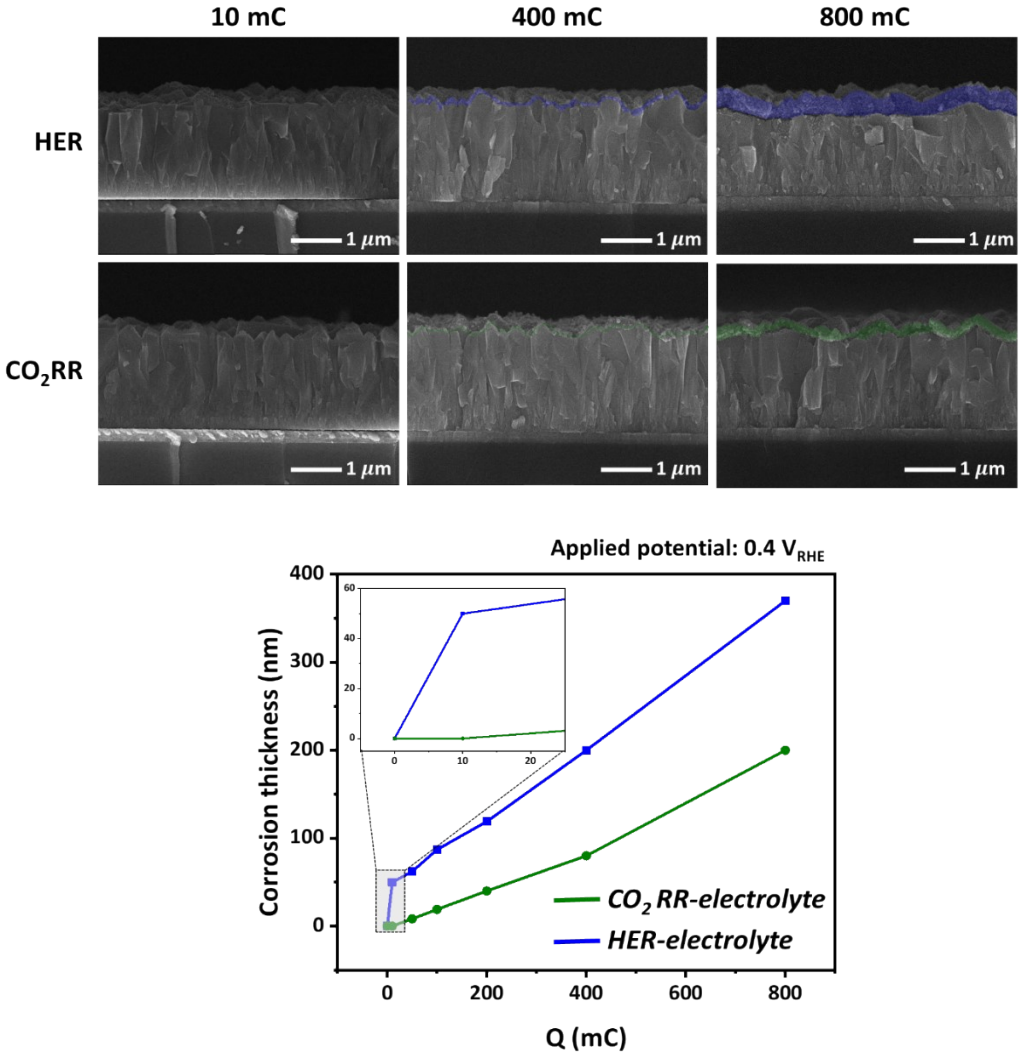

Fig. S8 Cu metal layer formed by photocorrosion on the surface depending on the amount of charge in HER (blue) and CO_2RR (green) solution (0.4 V_{RHE}). The inset graph is an enlargement of the gray box area.

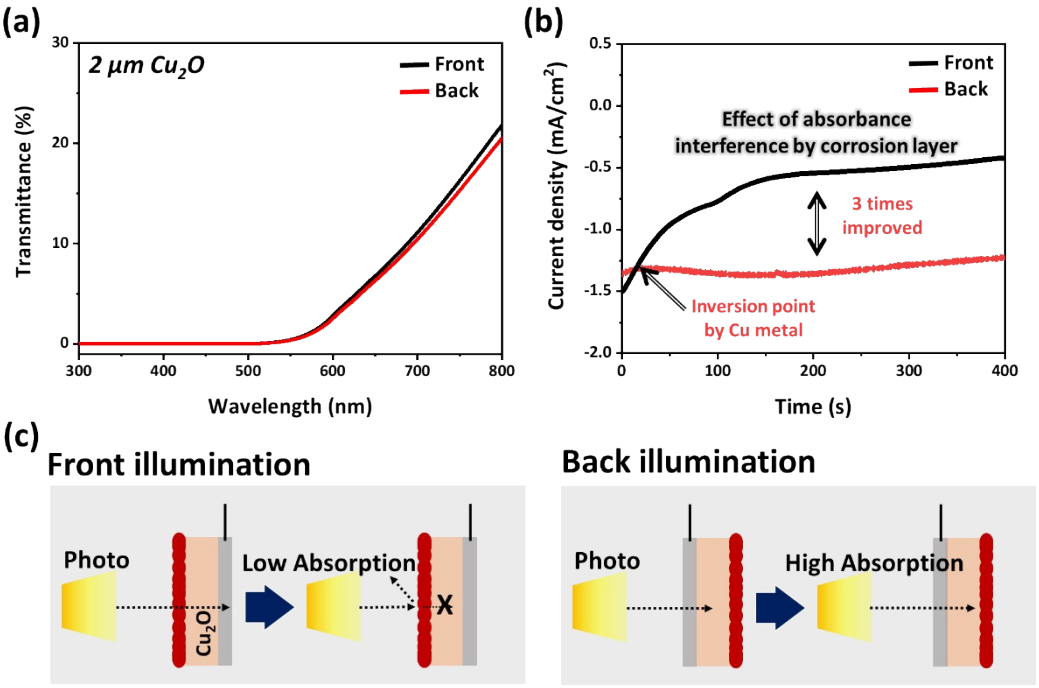

Fig. S9 (a) UV/VIS spectrophotometer and (b) I-t curve of back and front illumination. (c) Schematic image of front and back illumination.

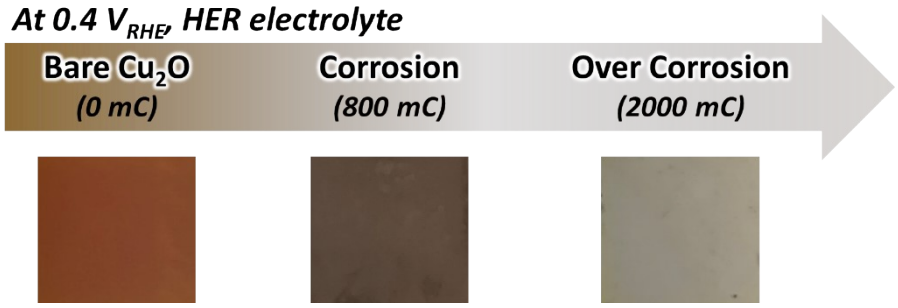

Fig. S10 Surface change of Cu_2O by continuous photocorrosion at 0, 800, and 2000 mC in HER solution (0.4 V_{RHE})

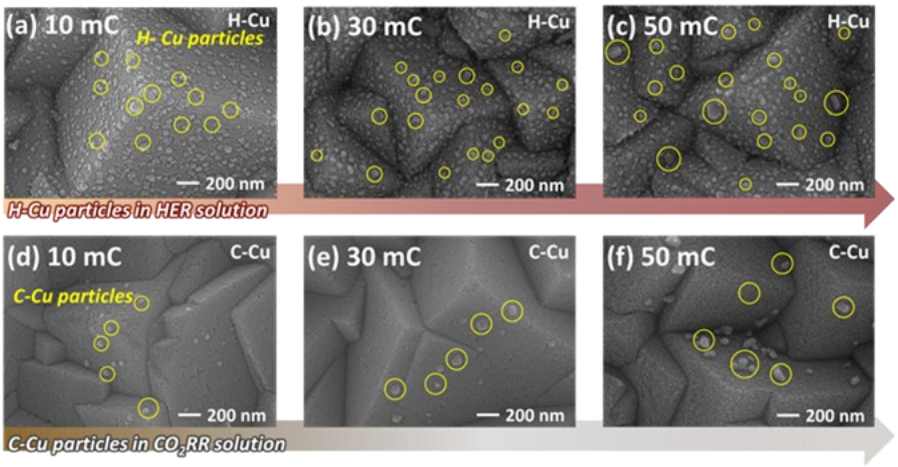

Fig. S11 Artificially controlled Cu-particles in (a) HER solution and (b) CO_2RR solution at 0 V_{RHE}.

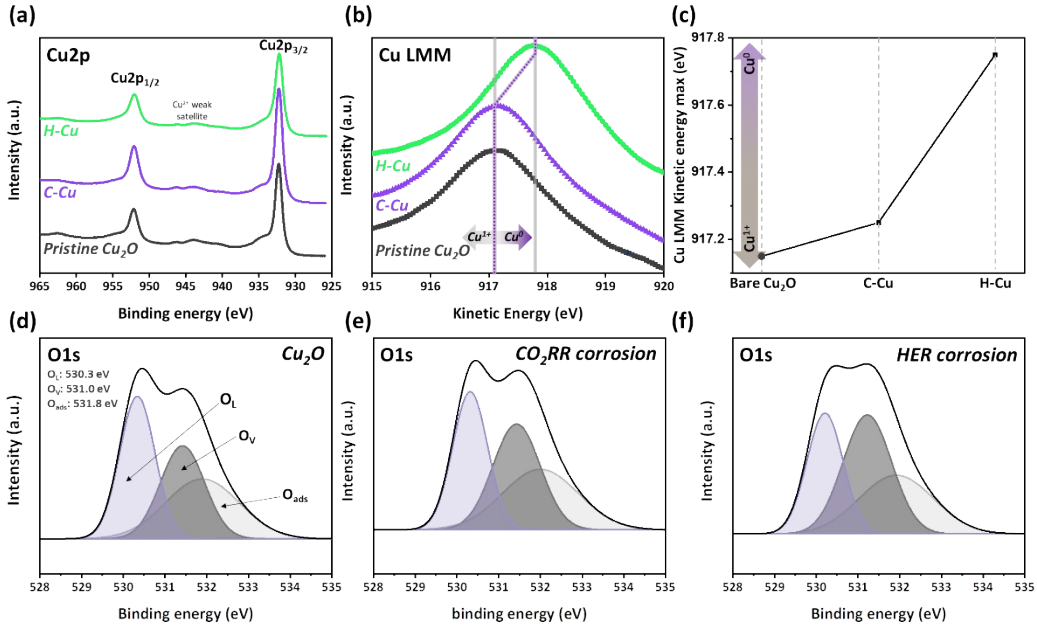

Fig. S12 X-ray photoemission spectroscopy (XPS) spectra of Cu2p and O1s (Al Kα=1486.6 eV). (a) Cu2p survey of pristine Cu_2O, C-Cu, and H-Cu. Cu 2p3/2 consists of Cu^0 = 932.61, Cu^+ = 932.28 eV, and Cu^{2+} = 934.7 ± 0.1 eV. (b) Cu LMM Auger spectra of pristine Cu_2O, C-Cu, and H-Cu. (c) Graph indicating the movement of the Cu LMM peak maximum. (d-f) Os1 survey of pristine Cu_2O, C-Cu, and H-Cu. O_L=Lattice Oxygen, O_V=Oxygen vacancy, O_{adh}=Adhesion oxygen (chemisorbed oxygen species).

XPS analysis was performed to study the copper and oxidation state of the Cu_2O surface after PEC measurement at 5 mC in the HER and CO_2 electrolytes (**Fig. S11a-f**). From the Cu2p spectra (**Fig S11a and S12**), it can clearly be seen that the three samples show typical spectra related to the Cu^+ oxidation state, with a very small and weak satellite corresponding to the Cu^{2+} state. The BE data used the C 1s (285.5 eV) peaks as a reference. The main peak of Cu 2p3/2 consisted of Cu^0 at 932.61, Cu^+ at 932.28 eV, and Cu^{2+} at 934.7 ± 0.1 eV. However, the peak at 932.3 eV can be assigned to either Cu^+ or Cu^0 because their binding energies almost overlap in the spectrum of Cu 2p3/2.[1,2] To further confirm this attribution, we also examined the CuL3M4.5M4.5 Auger peaks, from which the modified Auger parameter can be calculated (**Fig S11b and S11c**). This parameter also allowed us to distinguish between Cu^+ and Cu^0, which show almost the same chemical shift in Cu2p. Based on the pristine Cu_2O peak, Cu_2O with C-Cu was slightly shifted, but in the case of Cu_2O with H-Cu, the maximum peak shifted by 0.6 eV. Here, greater chemical shifts were observed for Cu LMM than for Cu2p. The presence of Cu^0 could be due to the partial photocorrosion of Cu_2O during CO_2RR. To further distinguish Cu^+ from Cu^0, it was necessary to split the O 1s spectrum. The presence of Cu_2O was also confirmed by the O 1s XPS spectrum (**Fig S11d-f**), in which the peak located at 530.6 eV is consistent with the value reported for O–Cu in Cu_2O. In addition, in **Fig S11f**, the increase in O vacancies of Cu_2O containing H-Cu is

expected to originate from the site where Cu metal is formed after oxygen is desorbed using the surface of Cu_2O as a seed.

References

1. J. J. Teo, Y. Chang and H. C. Zeng, *Langmuir*, 2006, **22**, 7369–7377.

2. J. Wang, C. Li, Y. Zhu, J. A. Boscoboinik and G. Zhou, *J. Phys. Chem. Lett.*, 2022, **13**, 5597–5604.

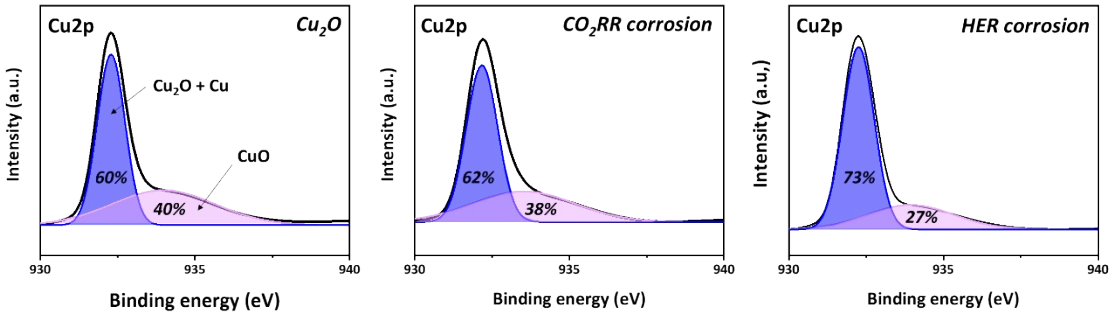

Fig. S13 XPS Cu2p HR survey. (a) Cu_2O. (b) Cu_2O/C-Cu. (c) Cu_2O/H-Cu. The purple area indicates the Cu_2O and Cu phases, and pink indicates the CuO phase.

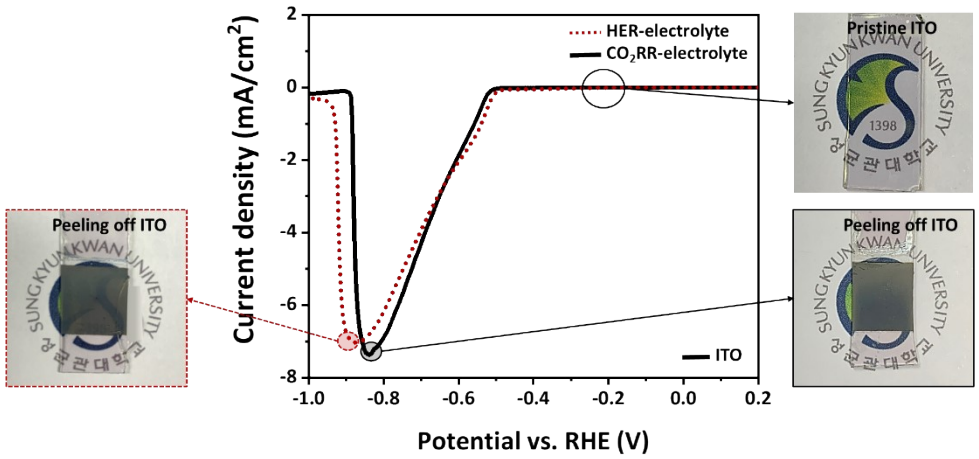

Fig. S14 LSV curves of ITO substrate in HER, CO_2RR solution under illuminated conditions, and electrode condition images at each indicated part.

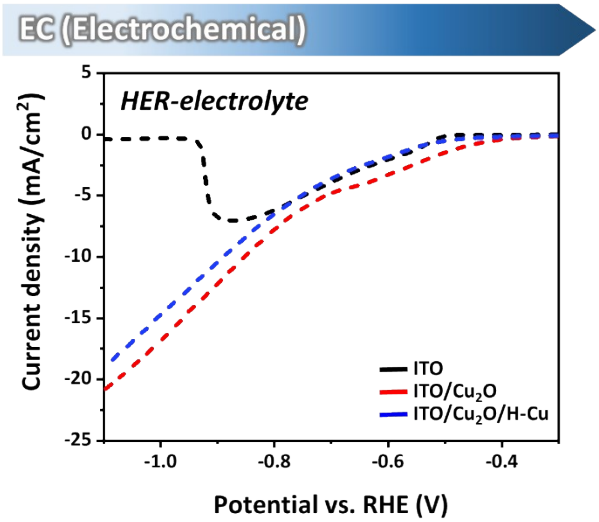

Fig. S15 LSV curves for ITO, ITO/Cu_2O, and ITO/Cu_2O/H-Cu in HER solution under no photo illumination.

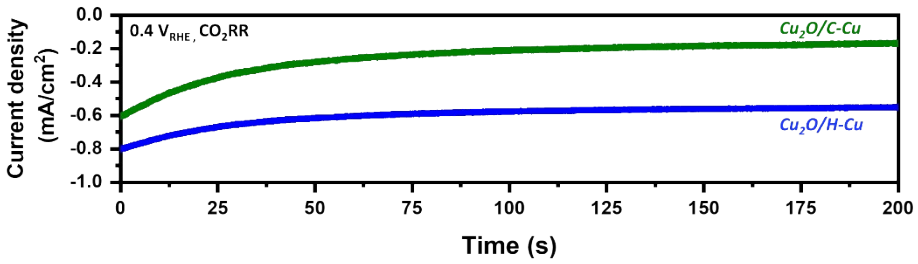

Fig. S16 Long-term stability of Cu_2O/H-Cu and Cu_2O/C-Cu photoelectrodes in 0.5 M $KHCO_3$ (0.4 V_{RHE}).

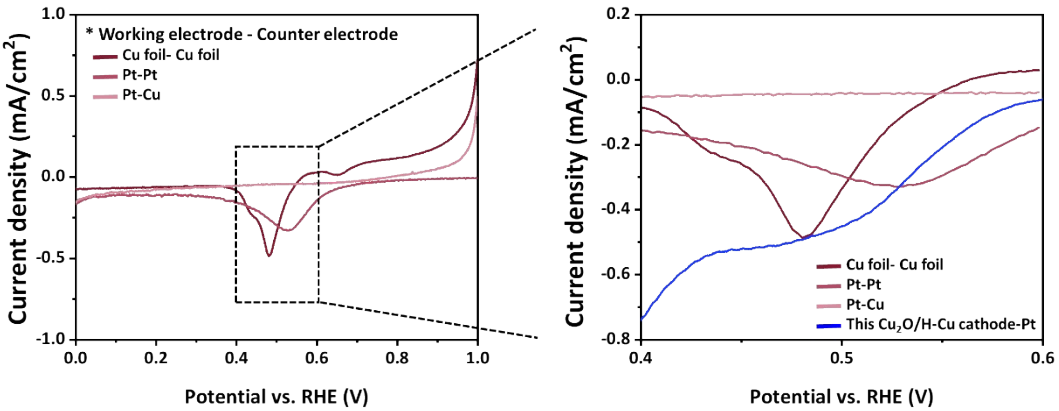

Fig. S17 Various electrodes conforming to overpotential in 0.5 M $KHCO_3$ and compared to Cu_2O/H-Cu cathode.

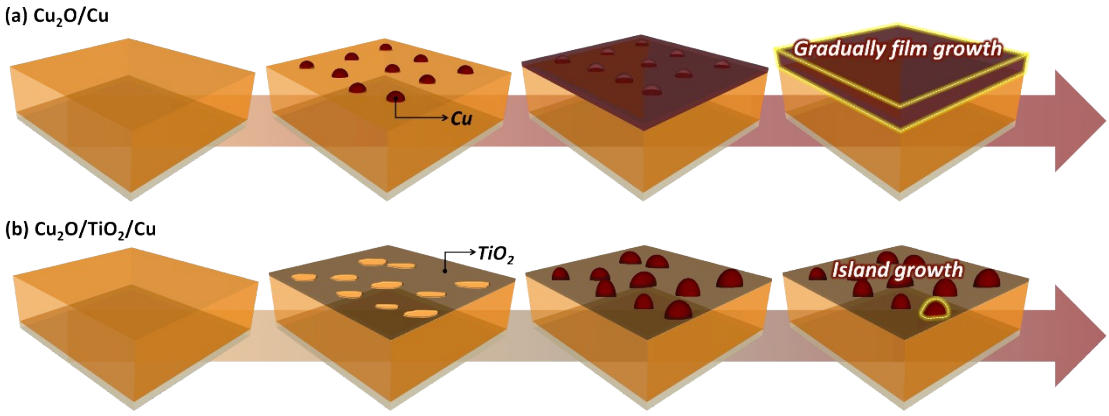

Fig. S18 Schematic image of (a) Cu_2O/Cu, Cu film formation as corrosion progresses and (b) $Cu_2O/TiO_2/Cu$ formation of island-grown Cu through (UT) TiO_2.

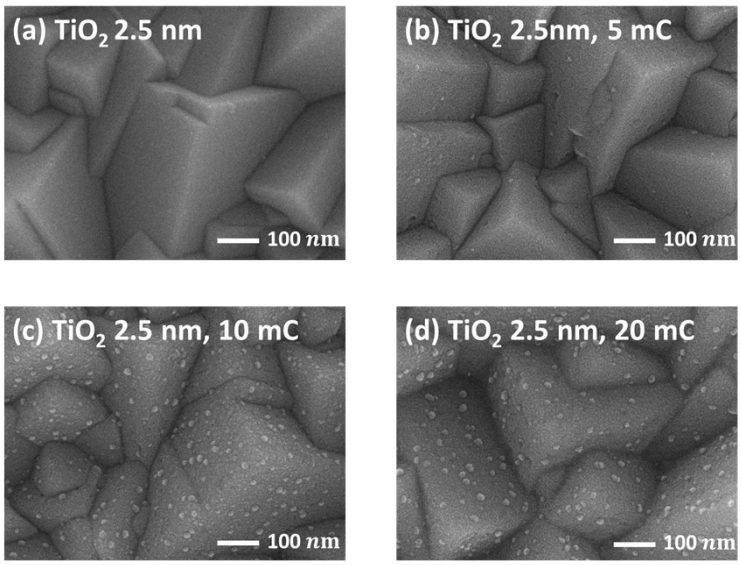

Fig. S19 H-Cu formation on 2.5 nm TiO_2 according to applied charge (5, 10, 20 mC).

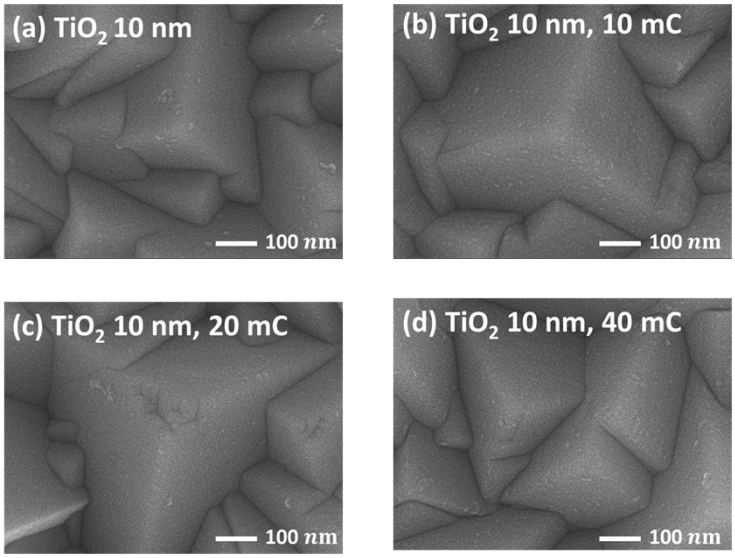

Fig. S20 H-Cu formation on 10 nm TiO_2 according to applied charge (10, 20, 40 mC).

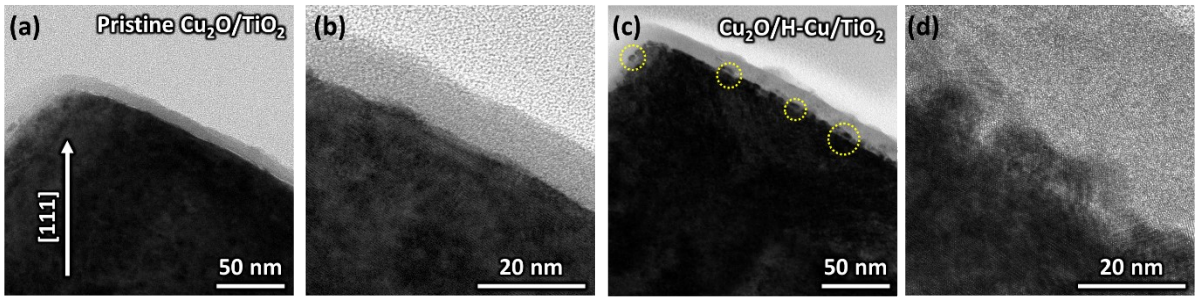

Fig. S21 TEM images of cathodes. (a, b) Cu_2O/TiO_2. (c, d) Cu_2O/H-Cu/TiO_2.

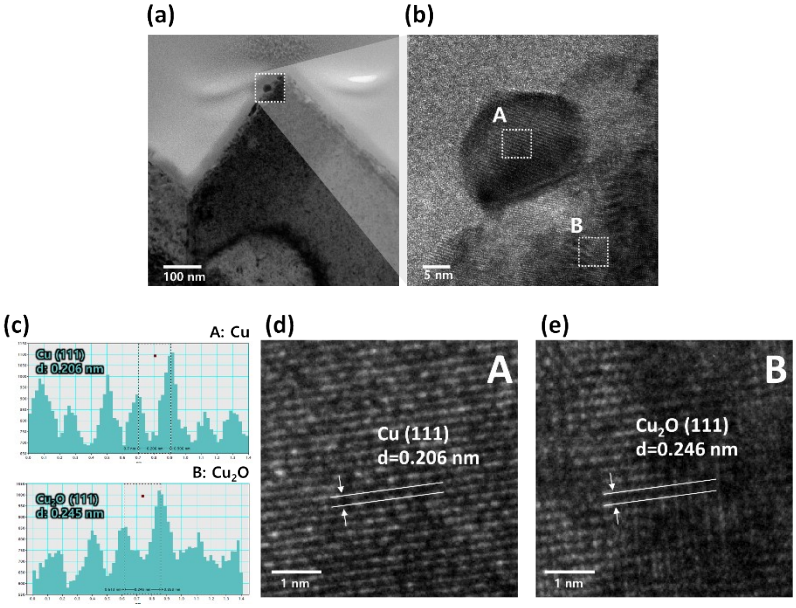

Fig. S22 HRTEM images of Cu_2O/C-Cu illustrating the formation of low-density metal catalysts over 20 nm in size.

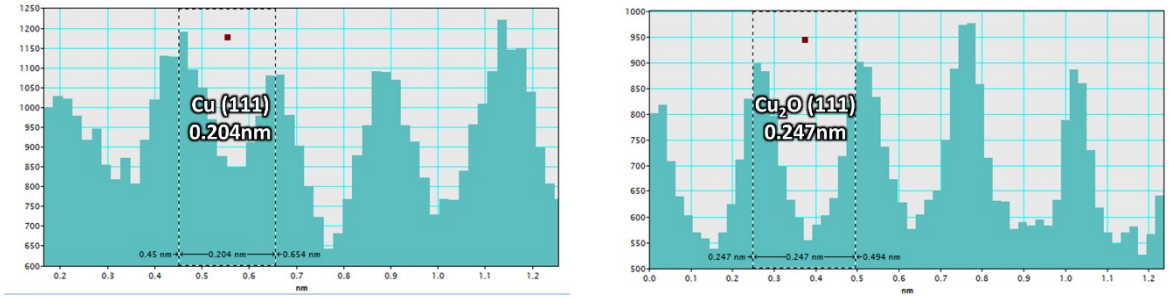

Fig. S23 Atomic distances in transmission electron microscopy (TEM) measurement results for Cu and Cu_2O.

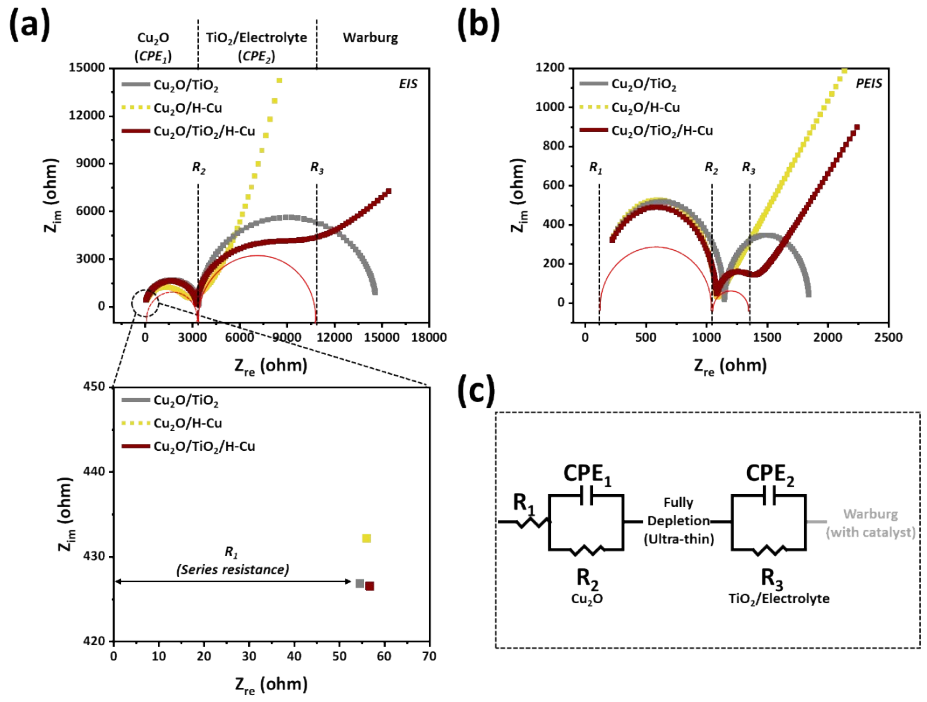

Fig. S24 Electrochemical analysis of Cu_2O/TiO_2 (grey), Cu_2O/H-Cu (yellow), and Cu_2O/TiO_2/H-Cu (red) at a dynamic potential (AC signal) of 0.4 V_{RHE}, a frequency ranging from 1 Hz to 1000 kHz, and an amplitude of 10 mV in 0.5 M $KHCO_3$; (a) electrochemical impedance spectra under dark conditions, and (b) photoelectrochemical impedance spectra under AM 1.5G simulated sunlight (100 mw cm^{-2}). (c) In the equivalent circuit, the electrochemical impedance spectroscopy results were fitted using the Z-view software.

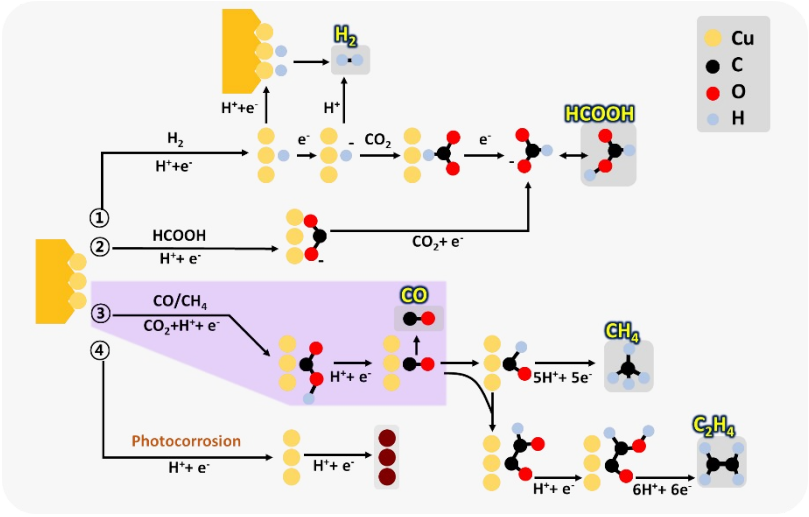

Fig. S25 Reaction pathways for CO_2RR toward different products of the Cu_2O/RM-TiO_2/H-Cu photocathode. This study highlights the dominant CO pathway during the photoelectrochemical CO_2 reduction reaction under illumination.

Table. S1 Photoelectrochemical (PEC) performance table.

Cell configuration Catalyst	Electrolyte	Product	Current density (mA/cm²) at 0.4 V_{RHE}	Ref.
Cu	**0.5 M $KHCO_3$**	**CO**	**1.57**	**This work**
Cu_2O NW/TiO_2/Cu	0.3 M $KHCO_3$	CH_3OH	1.1	[1]
Cu_2O/MOF-$Cu_3(BTC)_2$	0.1 M acetonitrile	CO	-0.8 (−1.97 $V_{Fc/Fc+}$)	[2]
Cu foil/ Cu_2O/CuO	0.1 M $KHCO_3$	CO, MeOH, Formic	0.3	[3]
NiO/Cu	K_2CO_3	HCOOH	~0.5	[4]
Cu foil/ Cu NW	0.1 M $KHCO_3$	CH_4	1	[5]
Cu_2O/TiO_2	MeCN, 0.1 M Bu4NPF6	CO	0.23 (at 0.6 V_{RHE})	[6]
$CuBi_2O_4$/TiO_2	0.1 M $KHCO_3$	CO	0.22 (at 0.6 V_{RHE})	[7]

References

1. K. Lee, S. Lee, H. Cho, S. Jeong, W. D. Kim, S. Lee and D. C. Lee, *J. Energy Chem.*, 2018, **27**, 264–270.

2. X. Deng, R. Li, S. Wu, L. Wang, J. Hu, J. Ma, W. Jiang, N. Zhang, X. Zheng, C. Gao, L. Wang, Q. Zhang, J. Zhu and Y. Xiong, *J. Am. Chem. Soc.*, 2019, **141**, 10924–10929.

3. D. H. Won, C. H. Choi, J. Chung and S. I. Woo, *Appl. Catal. B Environ.*, 2014, **158**–**159**, 217–223.

4. J. S. Duchene, G. Tagliabue, A. J. Welch, X. Li, W. H. Cheng and H. A. Atwater, *Nano Lett.*, 2020, **20**, 2348–2358.

5. Q. Wang, Y. Zhang, Y. Liu, K. Wang, W. Qiu, L. Chen, W. Li and J. Li, *J. Electroanal. Chem.*, 2022, **912**,116252.

6. M. Schreier, J. Luo, P. Gao, T. Moehl, M. T. Mayer and M. Grätzel, *J. Am. Chem. Soc.*, 2016, **138**, 1938–1946.

7. Y. Wang, H. Wang and T. He, *Chemosphere*, 2021, **264**, 128508.